ACS EARTH AND SPACE CHEMISTRY

http://pubs.acs.org/journal/aesccq

Article

Mixed Quantum/Classical Theory for Collisional Quenching of PAHs in the Interstellar Media

Bikramaditya Mandal, Carolin Joy, Alexander Semenov, and Dmitri Babikov*

Cite This: *ACS Earth Space Chem.* 2022, 6, 521−529

Read Online

ACCESS | Metrics & More | Article Recommendations | Supporting Information

ABSTRACT: A computationally affordable methodology is developed to predict cross sections and rate coefficients for collisional quenching and excitation of large molecules in space, such as PAHs. Mixed quantum/classical theory of inelastic scattering (MQCT) is applied, in which quantum state-to-state transitions between the internal states of the molecule are described using a time-dependent Schrodinger equation, while the scattering of collision partners is described classically using mean-field trajectories. To boost the numerical performance even further, a decoupling scheme for the equations of motion and a Monte Carlo sampling of the initial conditions are implemented. The method is applied to compute cross sections for rotational excitation and quenching of a benzene molecule (C_6H_6) by collisions with He atoms in a broad range of energies, using a very large basis set of rotational eigenstates up to $j = 60$, and close to one million nonzero matrix elements for state-to-state transitions. The properties of collision cross sections for C_6H_6 + He are reported and discussed. The accuracy of the approximations is rigorously tested and is found to be suitable for astrophysical/astrochemical simulations. The method and code developed here can be employed to generate a database of collisional quenching rate coefficients for PAHs and other large molecules, such as iCOMs, or for molecule−molecule collisions in cometary comas.

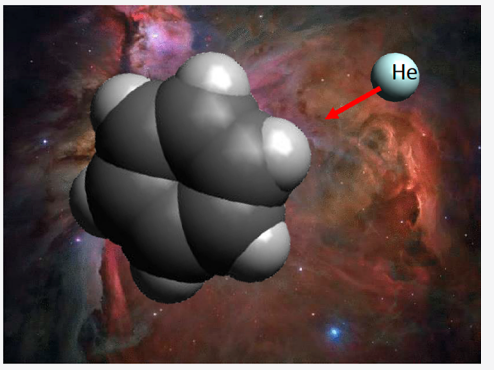

KEYWORDS: *inelastic scattering, rotational excitation, state-to-state transitions, rotational states, inelastic cross sections, MQCT, benzene, C_6H_6*

INTRODUCTION

Inelastic collisions between molecules and background gases, such as He and H_2, play important roles in the interstellar media, because these energy-transfer processes contribute to the rates of gas cooling and thus influence the processes of formation of prestellar cores and protoplanetary disks.[1−3] Moreover, the observation of molecular transitions in space provides a unique tool for a quantitative analysis of physical conditions in various astrochemical environments, permitting constraint of the temperature, density, and chemical composition of the emitting gas, which in turn helps to describe the evolution of these objects.[4−6] Quantitative analysis in these and other applications is only possible if the rate coefficients (or cross sections) are known for the collisional quenching and excitation of astrochemically important molecules.[7] This information becomes critical for the environments that are far from thermodynamic equilibrium, such as in protostellar shocks and bipolar jets (chemically reach outflows of forming stars).[8−10]

Experimental measurements of inelastic collision cross sections in the laboratory are possible but are challenging;[11] thus, astronomers often rely on the results of computational modeling of these processes. Unfortunately, classical trajectory methods, often employed to predict the rates of chemical reactions, are not directly suitable for the spectroscopic applications mentioned above, where transitions between the individual quantized states of molecules (rotational, vibrational) are considered. On the other extreme, the full-quantum mechanical calculations of molecular state-to-state transitions are affordable only for the simplest molecules (diatomic and triatomic)[12−15] and the lightest collision partners (diatomic at most). For small polyatomic molecules such calculations are affordable only in the very-low-energy regime.[16,17] As the complexity of the astrochemical environments grows, with more complex, larger, and heavier molecules being detected in space, one starts begging for a practical computational tool, capable of predicting the rates of molecular excitation and quenching in a satisfactory manner. Among the largest targeted molecules, one finds interstellar complex organic molecules (iCOMs),[18,19] unsaturated linear carbon chains,[20−22] and polycyclic aromatic hydrocarbons (PAHs).[23] The last group

Special Issue: Chemical Complexity in Planetary Systems

Received: November 28, 2021
Revised: January 28, 2022
Accepted: February 16, 2022
Published: February 24, 2022

spans an impressive range of sizes and masses, going from smaller molecules with well-known shapes (such as naphthalene, anthracene, etc.) all the way up to carbon sheets in the nanometer size range (several hundred atoms),[24,25] where even the identification of relevant isomers becomes challenging. How can we possibly solve the inelastic scattering problem for at least some of these targets?

During the past decade we developed a mixed quantum/classical approach for the description of molecule + atom and molecule + molecule collisions.[26−31] In our method the internal (rotational and vibrational) states of molecules are treated quantum mechanically, which permits a prediction of observables for quantum transitions, such as state-to-state specific cross sections. At the same time, the translational motion of collision partners is described classically using the mean-field trajectories, which captures the most important information about the scattering process, enabling massive parallelism and thus offering a very substantial computational advantage. We showed that the mixed quantum/classical theory (MQCT) is quite accurate for small molecules (when the full-quantum results are available for comparison)[32−34] and remains computationally affordable even for the largest systems ever studied in this context, such as collisional excitation of methyl formate by helium (CH_3COOH + He)[26] or collisional quenching in water vapor (H_2O + H_2O)[35,36] in cometary comas. The first user-ready version of our code, named MQCT, was recently made available to the community.[37]

In this paper our goal is to make the first step in the application of our theory and code to the collisional quenching of PAHs, by carrying out MQCT calculations for the smallest member of this group, the benzene molecule, colliding with a helium atom: C_6H_6 + He. For this, we compute cross sections for rotational excitation and quenching of benzene by helium in a broad range of collision energies using a large rotational basis set, up to $j_k = 60_{60}$. Quantum propensity rules are determined and discussed, and an efficient simplified approach for such calculations is developed. To the best of our knowledge, no quantum mechanical calculations of inelastic state-to-state cross sections for benzene have ever been attempted before.

MQCT METHODOLOGY

Here we briefly summarize the equations of motion propagated within framework of the mixed quantum/classical theory. A rigorous derivation of these formulas is available in the literature.[26−36]

The relative motion of two collision partners is described classically by vector $\vec{R}$ in the laboratory-fixed reference frame that connects their centers of mass. The length R of this vector and its azimuthal angle Φ (related to the deflection angle) evolve according to the following classical-like equations of motion[29,30]

$$\dot{R} = \frac{P_R}{\mu} \tag{1}$$

$$\dot{\Phi} = \frac{P_\Phi}{\mu R^2} \tag{2}$$

$$\dot{P}_R = -\sum_n \sum_{n'} e^{i\varepsilon_n^{n'} t} \sum_m \frac{\partial M_n^{n'}}{\partial R} a_{mn'}^* a_{mn} + \frac{P_\Phi^2}{\mu R^3} \tag{3}$$

$$\begin{aligned}\dot{P}_\Phi = -i \sum_n \sum_{n'} e^{i\varepsilon_n^{n'} t} \sum_m M_n^{n'} \\ \times [a_{m-1,n'}^* a_{mn} \sqrt{j'(j'+1) - m(m-1)} \\ + a_{m+1,n'}^* a_{mn} \sqrt{j'(j'+1) - m(m+1)} \\ - a_{mn'}^* a_{m-1,n} \sqrt{j(j+1) - m(m-1)} \\ - a_{mn'}^* a_{m+1,n} \sqrt{j(j+1) - m(m+1)}\,]/2\end{aligned} \tag{4}$$

where P_R and P_Φ are two generalized momenta associated with R and Φ.

In these formulas $\varepsilon_n^{n'}$ describes energy differences between the initial (lower index, unprimed) and the final (upper index, primed) internal states of the system: e.g., rotational or rovibrational states with energies E_n and $E_{n'}$. The index m labels projections of the total molecular angular momentum j onto the molecule−quencher axis $\vec{R}$ (which is the quantization axis z in the body-fixed reference frame). Multiple sums in eqs 3 and 4 go over all quantum states of the system. The time evolution of probability amplitudes $a_{mn}(t)$ for these molecular quantum states is described in the body-fixed reference frame, tied to the molecule−molecule vector $\vec{R}$, and is given by the following quantum-like system of coupled equations:[29,30]

$$\begin{aligned}\dot{a}_{mn} = -i \sum_{n'} e^{i\varepsilon_n^{n'} t} \sum_m M_{n'}^n a_{mn'} \\ - i\dot{\Phi}[a_{m-1,n} \sqrt{j(j+1) - m(m-1)} \\ + a_{m+1,n} \sqrt{j(j+1) - m(m+1)}\,]/2\end{aligned} \tag{5}$$

The second term in eq 5 describes transitions between the rotational states with $\Delta m = \pm 1$, driven by the classical orbital angular velocity $\dot{\Phi}$, which is the Coriolis coupling effect. The first term in eq 5 includes the potential coupling matrix $M_{n'}^n$ that depends parametrically on R (omitted for clarity). This matrix is real-valued time-independent and is diagonal in m (also omitted for clarity):

$$M_n^{n'}(R) = \langle \Psi_{n'}(\Lambda) | V(R, \Lambda) | \Psi_n(\Lambda) \rangle \tag{6}$$

The wave functions $\Psi_n(\Lambda)$ and $\Psi_{n'}(\Lambda)$ correspond to the initial and final states, respectively. They describe rotations of the molecule relative to the molecule−quencher axis R using a set of Euler angles $\Lambda = \{\alpha,\beta,\gamma\}$. In particular, for symmetric-top rotor molecules (such as benzene), the rotational states of given parity p (+ or −) are used to represent the basis set of molecular eigenstates

$$\Psi_{k,m}^{j,p}(\Lambda) = \sqrt{\frac{2j+1}{16\pi^2(1+\delta_{k0})}} [D_{+k,m}^j(\Lambda) \pm D_{-k,m}^j(\Lambda)] \tag{7}$$

where the usual Wigner D-functions are used but k is non-negative. The integrals of eq 6 are computed numerically using a multidimensional quadrature over angles Λ, for a grid of points R_i along the molecule−quencher distance R. When the trajectories are propagated, these precomputed values of $M_{n'}^n(R_i)$ are splined to give a smooth continuous dependence of $M_{n'}^n(R)$. It should be stressed that since the rovibrational motion of the molecule is treated quantum mechanically, the so-called "leakage" of zero-point energy (known to cause serious problems in the purely classical trajectory simulations) does not happen in the mixed quantum/classical calculations, where these internal states are quantized.

https://doi.org/10.1021/acsearthspacechem.1c00418
ACS Earth Space Chem. 2022, 6, 521−529

The equations of motion (eqs 1−5) are propagated through the interaction region and the values of inelastic transition cross sections are computed from the final probability amplitudes as[38]

$$\sigma_{n\to n'} = \frac{\pi}{(2j+1)k^2}\sum_{J=0}^{J_{max}}(2J+1)\sum_{m=-j}^{j}\sum_{m'=-j'}^{j'}|a^{(i)}_{m'n'}|^2 \quad (8)$$

This expression includes the usual sum over final and average over initial values of m' and m, respectively in the ranges determined by the final and initial values of molecular angular momenta j' and j, respectively that correspond to the final and initial states n' and n (in general, they can be rovibrational states). The outer sum is over the total angular momentum of the molecule−quencher system varied through the range $0 \le J \le J_{max}$; thus, J_{max} is a convergence parameter, just as in the full-quantum methods. The index i labels trajectories propagated for each initial state m of given j and for each value of the orbital angular momentum of collision l that changes through the range $|J - j| \le l \le J + j$, for each J. The value of l determines classical initial conditions for angular momentum, $P_\Phi = \hbar\sqrt{l(l+1)}$. The radial component of momentum P_R is set to satisfy the energy balance $P^2 = P_R^2 + P_\Phi^2/R^2$, where $P = \sqrt{2\mu U}$ is the total initial momentum related to the kinetic energy U of trajectory. The classical impact parameter b can be obtained from $P_\Phi = bP$. Thus, the impact parameter b is related to l but also depends on the energy and reduced mass of the system: $b = \hbar\sqrt{l(l+1)/(2\mu U)}$. Although a classical impact parameter is not used anywhere in the equations of motion, it is a useful property for setting up the initial conditions.

In theory, the propagation of each trajectory of this "batch" is required only if the differential and/or elastic cross sections are needed, since those are sensitive to the quantum phase shifts (not discussed here; see ref 38). If only the integral inelastic transition cross sections are of interest, as is the case here, the sampling of initial conditions can be replaced by a more efficient multidimensional Monte Carlo procedure as follows: draw randomly and uniformly the initial m from the range $-j \le m \le j$, draw the initial J value from the range $0 \le J \le J_{max}$, and finally draw the value of l from the range $|J - j| \le l \le J + j$ and use these random numbers to set up the trajectory i. The cross section is computed as an average over the sample using

$$\sigma_{n\to n'} = \frac{\pi}{k^2}\cdot\frac{J_{max}}{N}\sum_{i=1}^{N}(2J^{(i)}+1)|a^{(i)}_{m'n'}|^2 \quad (9)$$

where the number of trajectories N in the random sample is another convergence parameter. Note that if the quencher is also a molecule, such as H_2, then two angular momenta are introduced for the initial state of the molecule−molecule system, j_1 and j_2, and the procedure starts with a random sampling of j_{12} from the range $|j_1 - j_2| \le j_{12} \le j_1 + j_2$, then a sampling m_{12} from the range $-j_{12} \le m_{12} \le j_{12}$, then a random initial J, and only then the initial value of l from the range $|J - j_{12}| \le l \le J + j_{12}$. This replaces a four-dimensional sampling of the initial conditions by one Monte Carlo sampling, which is very efficient.

Even more computational speed can be obtained by decoupling[28] the propagation of quantum eq 5 from the classical eqs 1−4. This can be done by first propagating the whole system of coupled eqs 1−5 together, but using a small basis set of the internal molecular states (to make these calculations fast). The probability amplitudes a_{mn} of the quantum states are disregarded after this first run, and only the evolution of the classical variables R, Φ, P_R, and P_Φ is recorded. During the second run the internal molecular basis set size is increased to the desired value, and only the quantum equation (5) for the evolution of probability amplitudes a_{mn} is propagated, using the values of classical variables saved during the first run. The limiting case of this approach, when the first run is done using only the basis set of degenerate m states of the initial j channel, corresponds to the rotationally adiabatic trajectory method, which we call AT-MQCT.[28] This method was found to be sufficiently accurate and very efficient for H_2O + H_2 and for H_2O + H_2O collisions and will be tested below for the C_6H_6 + He collisions. Note that AT-MQCT can be used in conjunction with the Monte Carlo sampling described above.

RESULTS

For these calculations we used an existing *ab initio* potential energy surface (PES) from the literature for the interaction of C_6H_6 with a He atom.[39] A 6-fold symmetry of the interaction potential leads to nonzero matrix elements only for transitions with $\Delta k = \pm 6$, where k is a projection of j on the symmetry axis of benzene (perpendicular to the plane of the molecule). Also, since the PES is symmetric with respect to the plane of the molecule, only the transitions with $\Delta j = \pm 2$ are allowed, just as in the case of a diatomic molecule. Therefore, for calculations in which the initial state is the rotational ground state $j_k^p = 0_0^+$ (where p is parity), we included in the rotational basis set only the states with $k = 0$, 6, 12, etc. (up to $k = j$) with even j values up to $j = 60$ and only the states of positive parity (+). This resulted in 176 nondegenerate quantum states in the basis set (channels). The rotational constants $A = B = 0.18960$ cm^{-1} and $C = 0.09480$ cm^{-1} were used for the oblate symmetric top model of benzene,[40] with the highest energy state $j_k^p = 60_0^+$ at 693.936 cm^{-1}. The inclusion of degenerate m states leads to a total of 14036 quantum states in the calculations and 970628 nonzero matrix elements for state-to-state transitions.

To ensure that symmetry properties were taken into account correctly, we also tried to include in the basis set all states (with all values of j and k and of both parities p) and, using a multidimensional quadrature, computed all state-to-state matrix elements. We found that for all transitions we neglected the matrix elements are indeed near numerical zero; thus, including these states would not lead to any state-to-state transitions anyway. Figure 1 gives several examples of nonzero diagonal and off-diagonal matrix elements for the C_6H_6 + He system. The diagonal matrix elements reflect a long-range interaction that extends far into the molecule−quencher distance, through $\sim 30a_0$. Therefore, the values of $R_{max} = 50a_0$ was used, which in conjunction with $b_{max} = R_{max}$ leads to $J_{max} = 125$ for the collision energy $U = 100$ cm^{-1}, $J_{max} = 397$ for the collision energy $U = 1000$ cm^{-1}, and $J_{max} = 1257$ for the collision energy $U = 10000$ cm^{-1}. Note that the full-quantum calculations of inelastic scattering would hardly be possible for these large values of J. From Figure 1 we also see that the off-diagonal matrix element for the $\Delta j = 2$ transition also exhibits a long-range behavior. This is due to a pronounced anisotropy of the PES for this system, which exhibits a potential well over 80 cm^{-1} deep at the symmetry axis (at the "poles") but is much shallower in the plane of the molecule (in the "equatorial"

https://doi.org/10.1021/acsearthspacechem.1c00418
ACS Earth Space Chem. 2022, 6, 521−529

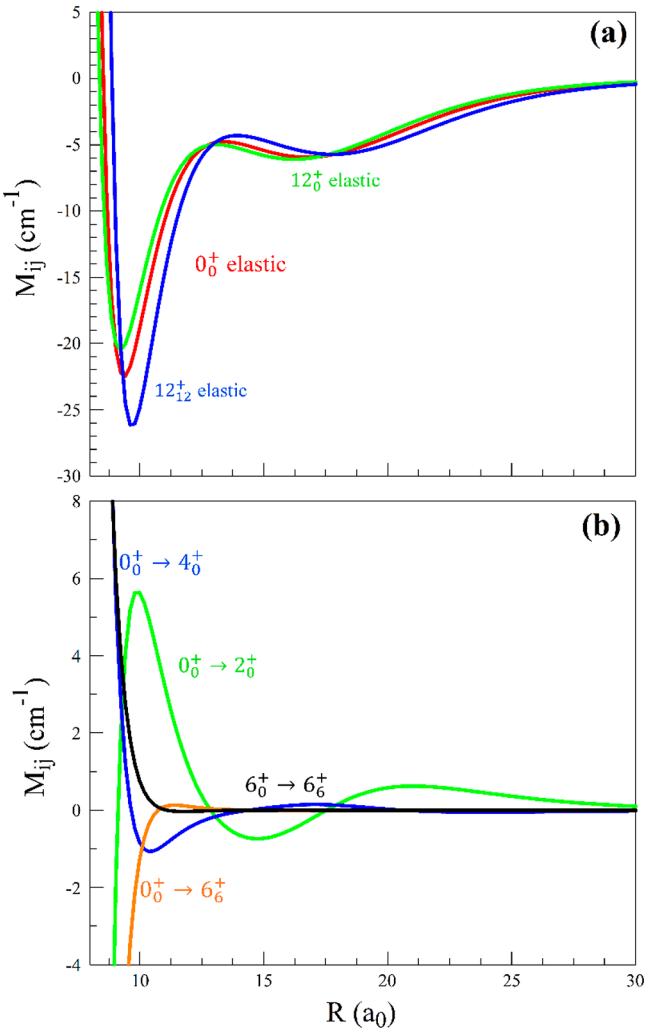

Figure 1. Several diagonal (a) and off-diagonal (b) matrix elements for the C_6H_6 + He system. A long-range interaction well is clearly seen. Inelastic transitions remain important up to the $R = 30a_0$ range of the molecule−quencher distances. Only the case of $m = 0$ is shown; the matrix elements for other values of m are similar.

plane). As we will see below, this polar anisotropy will result in a long ladder of $\Delta j = 2$ transitions.

Our standard full-coupled CC-MQCT calculations, which are expected to serve as a reference and thus need to be perfectly converged, were carried out in the usual way, using a fourth-order Runge−Kutta integrator with a constant time step set to a rather small value, $\Delta t = 50$ a.u. The convergence of the approximate AT-MQCT calculations with the adiabatic step-size predictor[28] was also rigorously checked, by varying the value of accuracy ϵ (see ref 28 for details). The results presented in Figure 3 are found to be entirely converged when $\epsilon = 10^{-3}$.

In the literature there is only one example of scattering calculations for the C_6H_6 + He system[41] using a simplified isotropic potential, which can only give the *elastic* cross section. Interestingly, the results of those calculations were found to be in good agreement with experimental results for the *total* cross section (reported in the same paper). This is quite possible, since all inelastic cross sections are much smaller than the elastic cross section (by at least 1 order of magnitude; see below) and because the experimental results were scaled to match the results of the calculations (as the experiment in ref 41 does not give the absolute values). Therefore, we decided to run, first of all, some comparison of our results *vs* those data available from the literature. In Figure 2 we present the

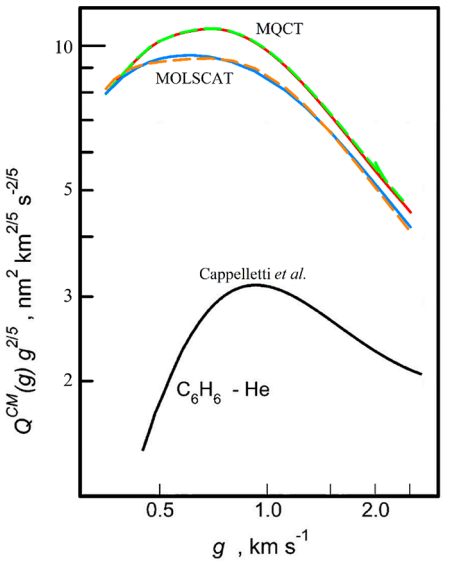

Figure 2. Dependence of elastic cross sections on the speed of collision, as in Figure 2 of ref 41. The black solid line is the result of ref 41, reproduced with permission. Solid red and blue lines show our results obtained using MQCT and MOLSCAT, respectively, for the initial state 30_0. Dashed green and orange lines represent our results obtained for the initial state 36_{24} with MQCT and MOLSCAT, respectively.

dependence of the elastic cross section on the speed of collision, replicated from ref 41. Those experiments were conducted with room-temperature C_6H_6 target molecules. Therefore, for our calculations of elastic cross sections, we have chosen several highly excited rotational states at an energy near 200 cm^{-1}, which corresponds to kT at 300 K. We found that the values of elastic cross sections for all such states are very similar. In Figure 2 we present the dependence of the elastic cross section for the 30_0^+ and 36_{24}^+ states of C_6H_6 at energies of 200.2 and 197.9 cm^{-1}, respectively. Note that one of them has $k = 0$, while the other has the very large $k = 24$; still, the dependences of elastic cross sections on the collision velocity are nearly identical. In order to mimic the elastic calculations of ref 41 by our MQCT calculations, we reduced the basis set to only one (elastic, initial) channel but included all degenerate m states. From Figure 2 we see that the positions of peaks, and the overall shapes of dependences, are very similar here and in ref 41, but the magnitudes are different by a factor of 3−4. This difference is likely to occur due to the fact that an approximate averaged potential was used in ref 41, while here we use an accurate PES that exhibits significant anisotropy.[39] Also, quite unfortunately, it is unknown what theoretical method was used in ref 41 for the calculations of scattering. In order to eliminate the possibility that something is wrong with our MQCT code, we caried out an additional set of elastic scattering calculations using the well-known full-quantum code MOLSCAT,[42] for the same states of benzene: 30_0^+ and 36_{24}^+ (such calculations become affordable if just one quantum state is included). These data are also presented in Figure 2. They are very similar to our MQCT results, with the maximum difference being ∼13% at low collision energies, which represents a successful test of our mixed quantum/classical methodology.

https://doi.org/10.1021/acsearthspacechem.1c00418
ACS Earth Space Chem. 2022, 6, 521−529

Next, we looked in detail at the rotational excitations from the ground state of the system, 0_0^+. Figure 3 in the main text

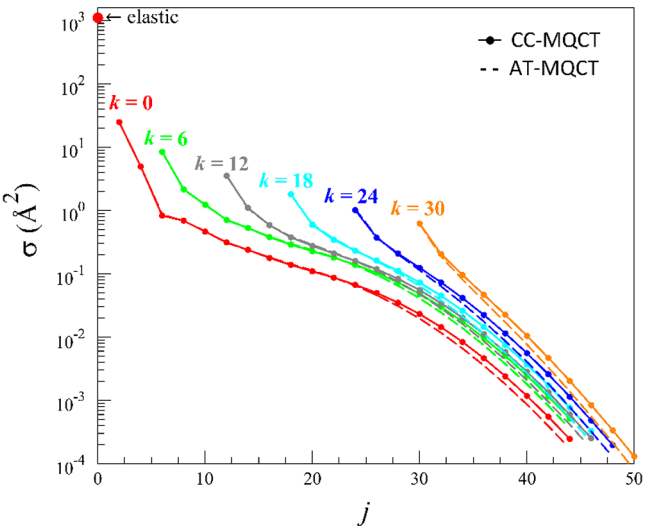

Figure 3. Comparison of results of the approximate AT-MQCT method (dashed line) against the full-coupled CC-MQCT calculations (solid line with symbols) for rotational excitation of the ground state 0_0^+ of C_6H_6 at a collision energy of 100 cm^{-1}. Quantum numbers j of the final rotational states are listed along the horizontal axis, while their quantum numbers k are indicated by various colors. The values of collision cross sections are plotted along the vertical axis using a log scale. The value of the elastic cross section is also shown.

and Figure S1 in the Supporting Information report cross sections for 200 state-to-state transitions, including the elastic channel, for the two values of collision energy U = 100 cm^{-1} and U = 1000 cm^{-1}, respectively. One can see that the results of the approximate AT-MQCT method (dashed lines) follow closely the trend of the benchmark CC-MQCT data (solid lines with symbols) through all transitions and all collision energies, systematically. We did not find even one transition where the adiabatic trajectory method would fail badly. Note that the values of cross sections in Figure 3 and Figure S1 vary through a range of 7 orders of magnitude. Still, the results of the approximate AT-MQCT method remain very close to the results of the full-coupled CC-MQCT method, even for very small cross sections.

In Figure 4 we present the error (in percent) of AT-MQCT cross sections relative to the CC-MQCT benchmark data, for the collision energy U = 100 cm^{-1}. The case of U = 1000 cm^{-1} is reported in Figure S2 in the Supporting Information. These data indicate that for larger, practically important cross sections (up to J = 24 or so) the difference between AT and CC versions of theory remains within 5% of the cross-section values. Only when the value of cross section drops by several orders of magnitude does the difference start to increase, reaching 40% for the weakest (basically negligible) transitions. However, even in this case the error of the AT method does not "explode". It grows linearly with J and remains tolerable. These results are encouraging and justify the use of an adiabatic trajectory approximation for this system. In what follows, the AT-MQCT version will be used. One advantage of AT-MQCT is the computational speed, which for this system is a factor of ~16 at U = 100 cm^{-1} and a factor of ~19 at U = 1000 cm^{-1}. These speed-up data were determined by running MQCT calculations on a Cray XC40 machine at the National

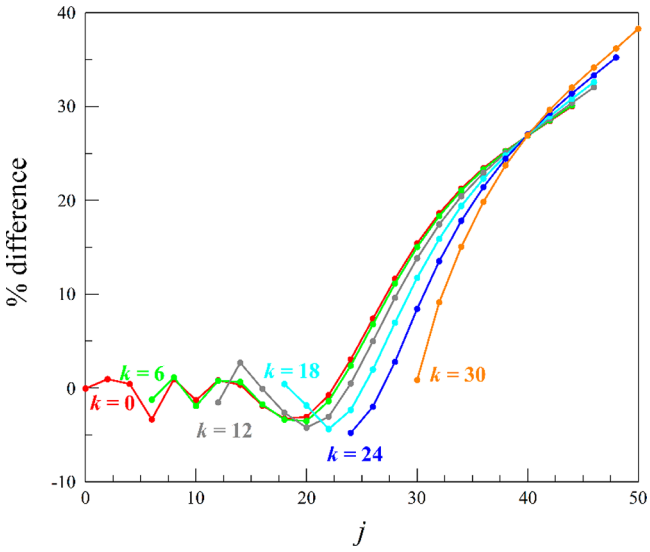

Figure 4. Relative deviation of AT-MQCT results from CC-MQCT results (percent error) for all cross sections presented in Figure 3 for the rotational excitation of the 0_0^+ state of C_6H_6 by He impact at a collision energy of 100 cm^{-1}. Quantum numbers j of the final rotational states are listed along the horizontal axis, while their quantum numbers k are indicated by various colors.

Energy Research Scientific Computing Center (Cori Supercomputer) using one Haswell node with 32 processors (2.3 GHz Intel Xeon E5-2698 v3). With this architecture, our AT-MQCT calculations took only 3.42 min (8.33 min) of the wall clock time at lower (higher) collision energy.

Another advantage of the adiabatic trajectory version of our theory is that it permits expanding MQCT calculations into the regime of low collision energies, dominated by quantum scattering resonances. While the trajectory-based MQCT method is not expected to capture every individual scattering resonance accurately, it permits mimicking the resonant behavior at low energies, on average. Figure 5 reports the energy dependence of several state-to-state transition cross sections in a broad range of collision energies, starting from the process threshold at low energies and going up to 10000 cm^{-1}. We see that slightly above the excitation threshold, and typically below 50 cm^{-1}, each curve passes through a series of peaks. Each peak is produced by one characteristic value of impact parameter that leads to the formation of a long-lived orbit, a phenomenon studied in detail in ref 38. In the full-coupled CC-MQCT version of theory such orbiting trajectories can be permanently trapped (due to inelastic energy exchange), while in the AT-MQCT version of theory they will typically leave after a few periods of orbiting, which permits us to run the final state analysis and compute inelastic cross sections at low collision energies, which is an important practical advantage.

It should be noted that not all cross sections in the high-energy part of Figure 5 are entirely converged with respect to the basis set size. Indeed, energies of the eigenstates in our rotational basis set reach, roughly, 700 cm^{-1}, which is a huge basis set when the small rotational constants of C_6H_6 are taken into account. Still, this is smaller than the range of collision energies in Figure 5. We tried to vary the basis set size and found that all important state-to-state transition cross sections are well converged up to a collision energy of ~2000 cm^{-1}. Above this energy, as one may notice from Figure 5, the energy

https://doi.org/10.1021/acsearthspacechem.1c00418
ACS Earth Space Chem. 2022, 6, 521−529

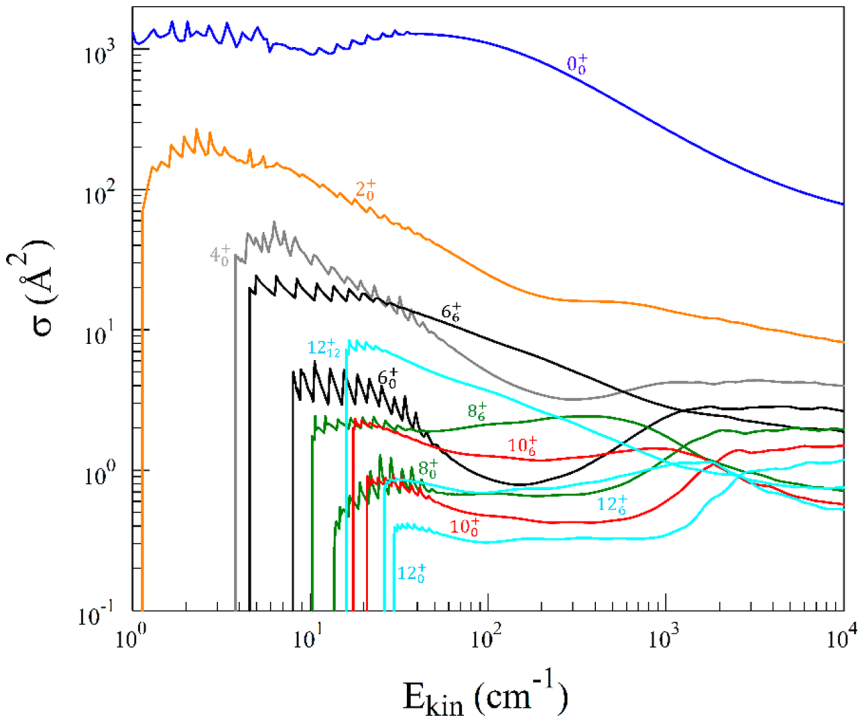

Figure 5. Energy dependence of excitation cross sections for several rotational states of C_6H_6 starting from the rotational ground state 0_0^+, colliding with a He atom. The dependence of the elastic cross section is also shown.

dependences of inelastic cross sections are not entirely smooth; they exhibit some (relatively small, residual) oscillations. These oscillations represent a vestige of an insufficient basis set size (at high energy). When the basis set size is increased, these oscillations vanish and the energy dependence becomes smooth, which is the behavior expected at high collision energies.

One important measure of the accuracy of the MQCT method is the deviation of state-to-state transition cross sections from the values that obey the principle of microscopic reversibility:

$$(2j + 1)\sigma_{j\to j'} = (2j' + 1)\sigma_{j'\to j} \quad (10)$$

It is known that while the full-quantum methods satisfy this condition automatically, the trajectory-based semiclassical methods often violate this relationship to some extent. Our MQCT method is not an exception. Therefore, the property of eq 10 has to be checked and, if needed, one of the known procedures has to be employed[36] to symmetrize the state-to-state transition matrix, before it can be used in the kinetics simulations. Figure 6a compares cross sections for the rotational $0_0^+ \rightarrow 10_6^+$ transition, as a function of energy computed directly (by excitation of the 0_0^+ initial state) with that computed indirectly (in the "reverse", using eq 10 and the data from the MQCT calculations of quenching $10_6^+ \rightarrow 0_0^+$ carried out separately). We see that, although the microscopic reversibility principle is not exactly satisfied, the two sets of results remain very close to each other through the entire range of collision energies, from $U = 1$ cm^{-1} to $U = 10000$ cm^{-1}. A similar behavior is seen in Figure 6a for the quenching $10_6^+ \rightarrow 0_0^+$ transition, which means that a meaningful symmetrization procedure can be carried out to enforce the microscopic reversibility principle in the final data produced by MQCT. Figure 6b gives the same information for transitions between two excited states, $10_6^+ \rightarrow 12_0^+$ and $12_0^+ \rightarrow 10_6^+$, and these data look similar to those of Figure 6a. Importantly, the deviation of MQCT results from the principle of microscopic reversibility is manageable and appears to decrease at higher collision energies, as expected for a trajectory-based method with a classical component. Figure 6c gives yet another example, for transitions between 2_0^+ and 10_6^+, where the difference between the direct and reverse calculations appears to be larger, particularly at low collision energies.

State-to-state cross sections for the quenching of several excited rotational states of C_6H_6 by He are presented in Figure 7 for the collision energy $U = 100$ cm^{-1}. The case of $U = 1000$ cm^{-1} is reported in Figure S3 in the Supporting Information. It should be mentioned that for the initial states with larger values of j the regular MQCT calculations are heavier, since we must propagate trajectories with all $2j + 1$ values of the initial quantum number m, to account for the second summation in eq 8, over $-j \le m \le j$. When the initial state corresponds to $j > 10$, the numerical cost of such calculations increases by at least 1 order of magnitude.

To overcome this problem, one can employ the random Monte Carlo sampling of initial conditions (over both m and l) and use eq 9 to compute cross sections. The data presented in Figure 7a demonstrate the performance of such a Monte Carlo sampling, within the AT-MQCT method, for the initial states 12_0^+ (circles), 12_6^+ (diamonds), and 12_{12}^+ (squares) of C_6H_6. In these calculations we reduced the maximum value of the impact parameter to $b_{max} = 25a_0$ and propagated only 100 randomly sampled trajectories, instead of ~1800 trajectories in the regular AT-MQCT calculations. We see that the results of random sampling (dashed lines, empty symbols) are close to the benchmark data of regular calculations (solid lines, filled symbols) systematically through all transitions and all collision regimes. Differences between the two sets of data, on average, are about 10% of cross-section values, which seems to be

https://doi.org/10.1021/acsearthspacechem.1c00418
ACS Earth Space Chem. 2022, 6, 521−529

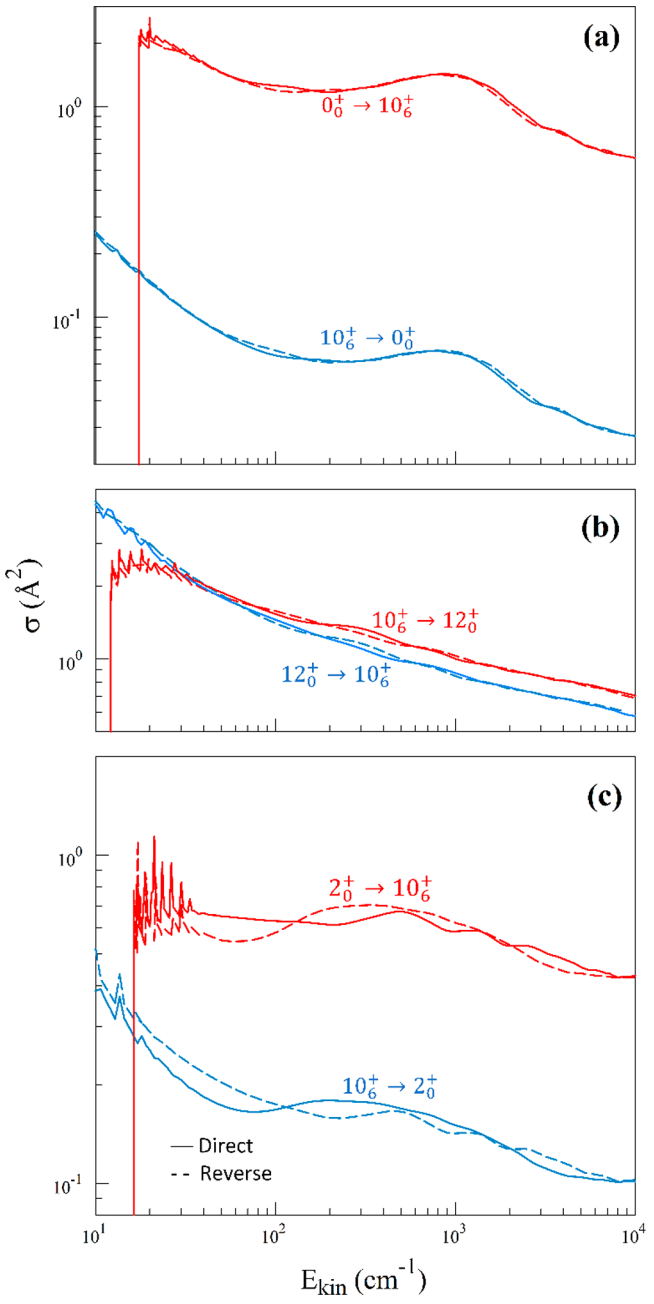

Figure 6. Test of the microscopic reversibility principle for transitions between several rotational states of C_6H_6 colliding with a He atom. The values of cross sections are plotted as a function of collision energy. The data obtained by direct calculations are shown by solid lines, while the results of "reverse" calculations are shown by dashed lines.

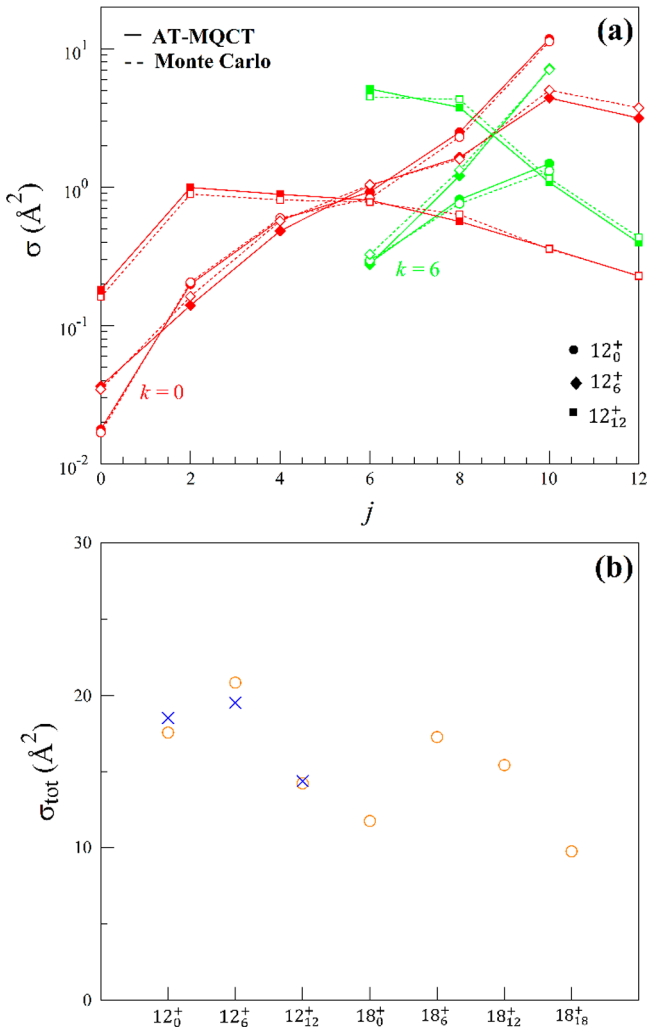

Figure 7. Individual state-to-state (a) and total (b) quenching cross sections for several initial states of C_6H_6 colliding with He atom at a kinetic energy of 100 cm^{-1}. The results of Monte Carlo sampling are shown by ○ symbols.

acceptable, especially if one takes into account a substantial speed-up, by a factor of close to 10.

In Figure 7b we present the total quenching cross sections for several initial states of C_6H_6, summed over the final j_k^+ states with j and/or k values smaller than those of the initial state. Here × symbols correspond to regular AT-MQCT calculations, whereas ○ symbols correspond to the Monte Carlo version. In addition to three $j = 12$ states, we included four $j = 18$ states: 18_0^+, 18_6^+, 18_{12}^+, and 18_{18}^+. For these we carried out only the Monte Carlo calculations with 100 trajectories, since regular calculations would be much more expensive. Computational speeding up of the Monte Carlo sampling has a significant advantage for the initial states with large values of angular momentum j and at higher collision energies U, since in these cases the "volume" of the sampling space is much larger, due to wide ranges of variations of the quantum numbers m and l. For example, for the initial state $j = 18$ the computational speed of Monte Carlo, relative to the regular calculations, is increased by a factor of about 15 at $U = 100$ cm^{-1} and close to 40 at $U = 1000$ cm^{-1}.

CONCLUSIONS

In this work we devised and tested a computationally affordable methodology to calculate cross sections and rate coefficients for collisional quenching and excitation of large interstellar molecules, such as PAHs. Our approach is based on the mixed quantum/classical theory of inelastic scattering, in which quantum state-to-state transitions between rotational states of the molecule are described using a time-dependent Schrodinger equation, while the scattering of collision partners is described classically, using the mean-field trajectory approach. Two more developments were undertaken to boost the numerical efficiency of the method. One is the

https://doi.org/10.1021/acsearthspacechem.1c00418
ACS Earth Space Chem. 2022, 6, 521−529

decoupling scheme, called the adiabatic trajectory approximation, that permits the propagation of equations for the evolution of classical and quantum degrees of freedom separately, which is much faster. The second trick is a multidimensional Monte Carlo sampling, which permits dramatically reducing the number of trajectories needed for numerical convergence, without sacrificing the physical rigor.

In this form, our method was applied to compute cross sections for collisional excitation and quenching of a benzene molecule (C_6H_6) by a He atom in a broad range of collision energies. Although benzene is the smallest member of the PAH family, these are the first-ever calculations of rotational state-to-state transitions for benzene and of any other PAH molecule, to the best of our knowledge. For C_6H_6, a very large basis set of close to 180 rotational eigenstates is needed (up to $j = 60$), which results in almost one million nonzero matrix elements for state-to-state transitions. Moreover, the system is characterized by a long-range interaction, which requires starting trajectories at a distance of ∼50 bohr. However, using our methodology and code, these huge calculations are still affordable. Overall, the accuracy of the adiabatic trajectory approximation was found to be acceptable, with errors within 5% of cross-section values for significant cross sections. A comparison of cross sections for excitation and quenching shows that some of them violate the principle of microscopic reversibility, but not significantly. Therefore, the state-to-state cross-section matrix can be symmetrized *a posterior*.

The success of our decoupling scheme (adiabatic trajectory version of MQCT) can be easily explained using Figures 3 and 5. They show that in the C_6H_6 + He system the elastic scattering cross section is at least 1 order of magnitude larger than any inelastic cross section, through a wide range of collision energies. This property is rather general; thus, AT-MQCT is expected to be reasonably accurate for many other molecular systems. An elastic cross section is governed by the isotropic part of the molecule−quencher interaction potential, while inelastic state-to-state transitions are driven by the anisotropic part of the PES. Therefore, one may expect that the worst-case scenario for our decoupling scheme would correspond to the molecules with highly anisotropic potentials, such as long carbon chains. This topic will be explored elsewhere.

All these findings are quite encouraging, which permits us to cautiously state that our method can be employed to generate a database of quenching rate coefficients, useful in the astrophysical modeling of C_6H_6 abundance in the interstellar media. Such calculations will be caried out soon, and the data will be deposited in the relevant databases such as BASECOL[43] and/or LAMDA.[44] New features of the mixed quantum/classical theory developed and tested here will be made available to the community in a new release of the MQCT suite of programs, planned for 2022.

■ ASSOCIATED CONTENT

Supporting Information

The Supporting Information is available free of charge at https://pubs.acs.org/doi/10.1021/acsearthspacechem.1c00418.

Comparison of results of the approximate AT-MQCT method against the full-coupled CC-MQCT calculations for C_6H_6 + He as in Figures 3 and 4, but at a collision energy of 1000 cm^{-1}, and a test of the Monte Carlo sampling for the individual state-to-state and the total quenching cross sections for several initial states of C_6H_6 colliding with a He atom, as in Figure 7, but for a kinetic energy of 1000 cm^{-1} (PDF)

■ AUTHOR INFORMATION

Corresponding Author

Dmitri Babikov − *Chemistry Department, Marquette University, Milwaukee, Wisconsin 53201-1881, United States;* orcid.org/0000-0002-4667-7645; Email: dmitri.babikov@mu.edu

Authors

Bikramaditya Mandal − *Chemistry Department, Marquette University, Milwaukee, Wisconsin 53201-1881, United States;* orcid.org/0000-0001-6682-0376

Carolin Joy − *Chemistry Department, Marquette University, Milwaukee, Wisconsin 53201-1881, United States*

Alexander Semenov − *Chemistry Department, Marquette University, Milwaukee, Wisconsin 53201-1881, United States;* Present Address: NOAA, Center for Weather and Climate Prediction, 5830 University Research Court, College Park, MD 20740, United States

Complete contact information is available at: https://pubs.acs.org/10.1021/acsearthspacechem.1c00418

Notes

The authors declare no competing financial interest.

■ ACKNOWLEDGMENTS

This research was supported in part by the NASA Astrophysics Program, grant number NNX17AH16G, and in part by the NSF Chemistry program, grant number CHE-2102465. B.M. acknowledges the support of the Eisch Fellowship at Marquette. We used resources of the National Energy Research Scientific Computing Center, which is supported by the Office of Science of the U.S. Department of Energy under Contract No. DE-AC02-5CH11231.

■ REFERENCES

(1) Tielens, A. G. G. M. *The Physics and Chemistry of the Interstellar Medium*; Cambridge University Press: 2005.

(2) Caselli, P.; Ceccarelli, C. Our Astrochemical Heritage. *Astron. Astrophys. Rev.* **2012**, *20*, 56.

(3) van Dishoeck, E. F.; Kristensen, L. E.; Benz, A. O.; Bergin, E. A.; Caselli, P.; Cernicharo, J.; Herpin, F.; Hogerheijde, M. R.; Johnstone, D.; Liseau, R.; et al. Water in Star-Forming Regions with the Herschel Space Observatory (WISH). I. Overview of Key Program and First Results. *Publ. Astron. Soc. Pacific* **2011**, *123*, 138.

(4) Roueff, E.; Lique, F. Molecular Excitation in the Interstellar Medium: Recent Advances in Collisional, Radiative, and Chemical Processes. *Chem. Rev.* **2013**, *113*, 8906−8938.

(5) Caux, E.; Kahane, C.; Castets, A.; Coutens, A.; Ceccarelli, C.; Bacmann, A.; Bisschop, S.; Bottinelli, S.; Comito, C.; Helmich, F. P.; et al. TIMASSS: The IRAS 16293−2422 Millimeter and Sub-millimeter Spectral Survey-I. Observations, Calibration, and Analysis of the Line Kinematics. *Astron. & Astrophys.* **2011**, *532*, A23.

(6) Vastel, C.; Ceccarelli, C.; Caux, E.; Coutens, A.; Cernicharo, J.; Bottinelli, S.; Demyk, K.; Faure, A.; Wiesenfeld, L.; Scribano, Y.; et al. Ortho-to-Para Ratio of Interstellar Heavy Water. *Astron. & Astrophys.* **2010**, *521*, L31.

(7) Hartmann, J.-M.; Boulet, C.; Robert, D. *Collisional Effects on Molecular Spectra: Laboratory Experiments and Models, Consequences for Applications*; Elsevier: 2008.
(8) Codella, C.; Lefloch, B.; Ceccarelli, C.; Cernicharo, J.; Caux, E.; Lorenzani, A.; Viti, S.; Hily-Blant, P.; Parise, B.; Maret, S.; et al. The CHESS Spectral Survey of Star Forming Regions: Peering into the Protostellar Shock L1157-B1-I. Shock Chemical Complexity. *Astron. & Astrophys.* **2010**, *518*, L112.
(9) Sakai, N.; Oya, Y.; Sakai, T.; Watanabe, Y.; Hirota, T.; Ceccarelli, C.; Kahane, C.; Lopez-Sepulcre, A.; Lefloch, B.; Vastel, C.; et al. A Chemical View of Protostellar-Disk Formation in L1527. *Astrophys. J. Lett.* **2014**, *791*, L38.
(10) Codella, C.; Ceccarelli, C.; Cabrit, S.; Gueth, F.; Podio, L.; Bachiller, R.; Fontani, F.; Gusdorf, A.; Lefloch, B.; Leurini, S.; et al. Water and Acetaldehyde in HH212: The First Hot Corino in Orion. *Astron. & Astrophys.* **2016**, *586*, L3.
(11) Wiesenfeld, L.; Faure, A.; Lique, F.; Dumouchel, N.; Feautrier, N.; Spielfiedel, A.; Scribano, Y. Analyzing Observations of Molecules in the ISM: Theoretical and Experimental Studies of Energy Transfer. *EAS Publ. Ser.* **2012**, *58*, 267−270.
(12) Daniel, F.; Dubernet, M.-L.; Grosjean, A. Rotational Excitation of 45 Levels of Ortho/Para-H_2O by Excited Ortho/Para-H_2 from 5 to 1500 K: State-to-State, Effective, and Thermalized Rate Coefficients. *Astron. & Astrophys.* **2011**, *536*, A76.
(13) Faure, A.; Wiesenfeld, L.; Scribano, Y.; Ceccarelli, C. Rotational Excitation of Mono-and Doubly-Deuterated Water by Hydrogen Molecules. *Mon. Not. R. Astron. Soc.* **2012**, *420*, 699−704.
(14) Denis-Alpizar, O.; Stoecklin, T.; Dutrey, A.; Guilloteau, S. Rotational Relaxation of HCO^+ and DCO^+ by Collision with H_2. *Mon. Not. R. Astron. Soc.* **2020**, *497*, 4276−4281.
(15) Ben Khalifa, M.; Quintas-Sánchez, E.; Dawes, R.; Hammami, K.; Wiesenfeld, L. Rotational Quenching of an Interstellar Gas Thermometer: CH_3CN···He Collisions. *Phys. Chem. Chem. Phys.* **2020**, *22*, 17494.
(16) Faure, A.; Szalewicz, K.; Wiesenfeld, L. Potential Energy Surface and Rotational Cross Sections for Methyl Formate Colliding with Helium. *J. Chem. Phys.* **2011**, *135*, 024301.
(17) Faure, A.; Dagdigian, P. J.; Rist, C.; Dawes, R.; Quintas-Sánchez, E.; Lique, F.; Hochlaf, M. Interaction of Chiral Propylene Oxide (CH_3CHCH_2O) with Helium: Potential Energy Surface and Scattering Calculations. *ACS Earth Sp. Chem.* **2019**, *3*, 964−972.
(18) Codella, C.; Ceccarelli, C.; Caselli, P.; Balucani, N.; Barone, V.; Fontani, F.; Lefloch, B.; Podio, L.; Viti, S.; Feng, S.; et al. Seeds of Life in Space (SOLIS)-II. Formamide in Protostellar Shocks: Evidence for Gas-Phase Formation. *Astron. & Astrophys.* **2017**, *605*, L3.
(19) Ceccarelli, C.; Caselli, P.; Fontani, F.; Neri, R.; López-Sepulcre, A.; Codella, C.; Feng, S.; Jiménez-Serra, I.; Lefloch, B.; Pineda, J. E.; et al. Seeds Of Life In Space (SOLIS): The Organic Composition Diversity at 300–1000 Au Scale in Solar-Type Star-Forming Regions. *Astrophys. J.* **2017**, *850*, 176.
(20) Remijan, A. J.; Hollis, J. M.; Snyder, L. E.; Jewell, P. R.; Lovas, F. J. Methyltriacetylene (CH_3C_6H) toward TMC-1: The Largest Detected Symmetric Top. *Astrophys. J. Lett.* **2006**, *643*, L37.
(21) Sakai, N.; Yamamoto, S. Warm Carbon-Chain Chemistry. *Chem. Rev.* **2013**, *113*, 8981−9015.
(22) Fontani, F.; Ceccarelli, C.; Favre, C.; Caselli, P.; Neri, R.; Sims, I. R.; Kahane, C.; Alves, F. O.; Balucani, N.; Bianchi, E.; et al. Seeds of Life in Space (SOLIS)-I. Carbon-Chain Growth in the Solar-Type Protocluster OMC2-FIR4. *Astron. \& Astrophys.* **2017**, *605*, A57.
(23) Tielens, A. G. G. M. Interstellar Polycyclic Aromatic Hydrocarbon Molecules. *Annu. Rev. Astron. Astrophys.* **2008**, *46*, 289−337.
(24) Mattioda, A. L.; Hudgins, D. M.; Boersma, C.; Bauschlicher, C. W., Jr; Ricca, A.; Cami, J.; Peeters, E.; de Armas, F. S.; Saborido, G. P.; Allamandola, L. J. The NASA Ames PAH IR Spectroscopic Database: The Laboratory Spectra. *Astrophys. J. Suppl. Ser.* **2020**, *251*, 22.
(25) Bauschlicher, C. W., Jr; Ricca, A.; Boersma, C.; Allamandola, L. J. The NASA Ames PAH IR Spectroscopic Database: Computational Version 3.00 with Updated Content and the Introduction of Multiple Scaling Factors. *Astrophys. J. Suppl. Ser.* **2018**, *234*, 32.
(26) Semenov, A.; Babikov, D. Mixed Quantum/Classical Approach for Description of Molecular Collisions in Astrophysical Environments. *J. Phys. Chem. Lett.* **2015**, *6*, 1854−1858.
(27) Babikov, D.; Semenov, A. Recent Advances in Development and Applications of the Mixed Quantum/Classical Theory for Inelastic Scattering. *J. Phys. Chem. A* **2016**, *120*, 319−331.
(28) Mandal, B.; Semenov, A.; Babikov, D. Adiabatic Trajectory Approximation within the Framework of Mixed Quantum/Classical Theory. *J. Phys. Chem. A* **2020**, *124*, 9877−9888.
(29) Semenov, A.; Babikov, D. Mixed Quantum/Classical Theory of Rotationally and Vibrationally Inelastic Scattering in Space-Fixed and Body-Fixed Reference Frames. *J. Chem. Phys.* **2013**, *139*, 174108.
(30) Semenov, A.; Babikov, D. Mixed Quantum/Classical Calculations of Total and Differential Elastic and Rotationally Inelastic Scattering Cross Sections for Light and Heavy Reduced Masses in a Broad Range of Collision Energies. *J. Chem. Phys.* **2014**, *140*, 044306.
(31) Semenov, A.; Babikov, D. Accurate Calculations of Rotationally Inelastic Scattering Cross Sections Using Mixed Quantum/Classical Theory. *J. Phys. Chem. Lett.* **2014**, *5*, 275−278.
(32) Semenov, A.; Babikov, D. Inelastic Scattering of Identical Molecules within Framework of the Mixed Quantum/Classical Theory: Application to Rotational Excitations in H_2 + H_2. *J. Phys. Chem. A* **2016**, *120*, 3861−3866.
(33) Semenov, A.; Babikov, D. Mixed Quantum/Classical Theory for Molecule–Molecule Inelastic Scattering: Derivations of Equations and Application to N_2+ H_2 System. *J. Phys. Chem. A* **2015**, *119*, 12329−12338.
(34) Semenov, A.; Dubernet, M.-L.; Babikov, D. Mixed Quantum/Classical Theory for Inelastic Scattering of Asymmetric-Top-Rotor + Atom in the Body-Fixed Reference Frame and Application to the H_2O + He System. *J. Chem. Phys.* **2014**, *141*, 114304.
(35) Semenov, A.; Babikov, D. MQCT. I. Inelastic Scattering of Two Asymmetric-Top Rotors with Application to H_2O+ H_2O. *J. Phys. Chem. A* **2017**, *121*, 4855−4867.
(36) Boursier, C.; Mandal, B.; Babikov, D.; Dubernet, M. L. New H_2O−H_2O Collisional Rate Coefficients for Cometary Applications. *Mon. Not. R. Astron. Soc.* **2020**, *498*, 5489−5497.
(37) Semenov, A.; Mandal, B.; Babikov, D. MQCT: User-Ready Program for Calculations of Inelastic Scattering of Two Molecules. *Comput. Phys. Commun.* **2020**, *252*, 107155.
(38) Mandal, B.; Semenov, A.; Babikov, D. Calculations of Differential Cross Sections Using Mixed Quantum/Classical Theory of Inelastic Scattering. *J. Phys. Chem. A* **2018**, *122*, 6157−6165.
(39) Lee, S.; Chung, J. S.; Felker, P. M.; López Cacheiro, J.; Fernández, B.; Bondo Pedersen, T.; Koch, H. Computational and Experimental Investigation of Intermolecular States and Forces in the Benzene–Helium van Der Waals Complex. *J. Chem. Phys.* **2003**, *119*, 12956−12964.
(40) Herzberg, G. *Electronic Spectra and Electronic Structure of Polyatomic Molecules*; van Nostrand: 1966; Vol. 3.
(41) Cappelletti, D.; Bartolomei, M.; Pirani, F.; Aquilanti, V. Molecular Beam Scattering Experiments on Benzene- Rare Gas Systems: Probing the Potential Energy Surfaces for the C_6H_6- He,- Ne, and- Ar Dimers. *J. Phys. Chem. A* **2002**, *106*, 10764−10772.
(42) Hutson, J. M.; Le Sueur, C. R. *MOLSCAT, BOUND, and FIELD, Ver. 2020.0*, 2020.
(43) Dubernet, M.-L.; Alexander, M. H.; Ba, Y. A.; Balakrishnan, N.; Balança, C.; Ceccarelli, C.; Cernicharo, J.; Daniel, F.; Dayou, F.; Doronin, M.; et al. BASECOL2012: A Collisional Database Repository and Web Service within the Virtual Atomic and Molecular Data Centre (VAMDC). *Astron. Astrophys.* **2013**, *553*, A50.
(44) Schöier, F. L.; van der Tak, F. F. S.; van Dishoeck, E. F.; Black, J. H. An Atomic and Molecular Database for Analysis of Submillimetre Line Observations. *Astron. \& Astrophys.* **2005**, *432*, 369−379.

https://doi.org/10.1021/acsearthspacechem.1c00418
ACS Earth Space Chem. 2022, 6, 521−529